



# Evolutionary repurposing of a sulfatase: A new Michaelis complex leads to efficient transition state charge offset

Charlotte M. Miton<sup>a,1</sup>, Stefanie Jonas<sup>a,2</sup>, Gerhard Fischer<sup>a,3</sup>, Fernanda Duarte<sup>b,3,4</sup>, Mark F. Mohamed<sup>a</sup>, Bert van Loo<sup>a,5</sup>, Bálint Kintses<sup>a,6</sup>, Shina C. L. Kamerlin<sup>b</sup>, Nobuhiko Tokuriki<sup>a,c</sup>, Marko Hyvönen<sup>a</sup>, and Florian Hoffelder<sup>a,7</sup>

<sup>a</sup>Department of Biochemistry, University of Cambridge, CB2 1GA Cambridge, United Kingdom; <sup>b</sup>Department of Chemistry, Biomediskt Centrum (BMC), Uppsala University, 751 23 Uppsala, Sweden; and <sup>c</sup>Michael Smith Laboratories, University of British Columbia, Vancouver, BC V6T 1Z4, Canada

Edited by Daniel Herschlag, Stanford University, Stanford, CA, and accepted by Editorial Board Member Michael A. Marletta May 31, 2018 (received for review January 31, 2018)

The recruitment and evolutionary optimization of promiscuous enzymes is key to the rapid adaptation of organisms to changing environments. Our understanding of the precise mechanisms underlying enzyme repurposing is, however, limited: What are the active-site features that enable the molecular recognition of multiple substrates with contrasting catalytic requirements? To gain insights into the molecular determinants of adaptation in promiscuous enzymes, we performed the laboratory evolution of an arylsulfatase to improve its initially weak phenylphosphonate hydrolase activity. The evolutionary trajectory led to a 100,000-fold enhancement of phenylphosphonate hydrolysis, while the native sulfate and promiscuous phosphate mono- and diester hydrolyses were only marginally affected ( $\leq 50$ -fold). Structural, kinetic, and in silico characterizations of the evolutionary intermediates revealed that two key mutations, T50A and M72V, locally reshaped the active site, improving access to the catalytic machinery for the phosphonate. Measured transition state (TS) charge changes along the trajectory suggest the creation of a new Michaelis complex (E•S, enzyme–substrate), with enhanced leaving group stabilization in the TS for the promiscuous phosphonate ( $\beta_{\text{leaving group}}$  from  $-1.08$  to  $-0.42$ ). Rather than altering the catalytic machinery, evolutionary repurposing was achieved by fine-tuning the molecular recognition of the phosphonate in the Michaelis complex, and by extension, also in the TS. This molecular scenario constitutes a mechanistic alternative to adaptation solely based on enzyme flexibility and conformational selection. Instead, rapid functional transitions between distinct chemical reactions rely on the high reactivity of permissive active-site architectures that allow multiple substrate binding modes.

catalytic promiscuity | directed evolution | linear free-energy relationship | phosphate transfer | enzyme–substrate complementarity

Increasing evidence indicates that many, if not most, enzymes are promiscuous (1, 2). Their ability to catalyze multiple chemically distinct reactions in addition to their primary function (3, 4) constitutes a functional repertoire from which they can be recruited (5–8) and further enhanced by mutations to facilitate organismal adaptation through functional innovation (9–12). For example, in microorganisms and plants, enzyme promiscuity has been shown to underlie a broad range of metabolic adaptations, from the emergence of antibiotic resistance (13), the synthesis of pigments, flavors, or defense molecules (14) to the bioremediation of anthropogenic chemicals (15). The study of promiscuous enzymes not only broadens our understanding of molecular recognition, but it also provides invaluable insights into how evolution alters these molecular interactions to achieve functional repurposing (16).

A series of laboratory evolution experiments “replayed” such functional transitions by successfully enhancing low-level promiscuous reactions to efficient catalytic activities, comparable to those of natural enzymes (17–22). These studies demonstrate that enzyme adaptation is not limited to mutations targeting key

catalytic residues but also occurs at the periphery of the catalytic machinery, even in positions as remote as the second and third shells of the active site (23). In studies examining detailed evolutionary transitions, function-altering mutations led to the displacement of a catalytic metal ion or the repositioning of a nucleophile (24–26). In further cases, the position of the catalytic residues remained unaltered, but other structural features, for

## Significance

The versatility of promiscuous enzymes plays a key role in the evolution of catalysts. This work addresses the molecular mechanism of repurposing a promiscuous enzyme by laboratory evolution and reveals that mutations distinct from the catalytic machinery reshaped the active site. Evolution fine-tuned binding of a previously disfavored Michaelis complex (E•S), repositioning the promiscuous substrate to enable better charge offset during leaving group departure in the transition state. The functional transition relies on maintaining the reactivity of existing catalytic groups in a permissive active-site architecture, able to accommodate multiple substrate binding modes, without requiring changes in conformational dynamics. Such a parsimonious route to higher efficiency illustrates a molecular scenario in which catalytic promiscuity facilitates short adaptive pathways of evolution.

Author contributions: C.M.M., S.J., F.D., S.C.L.K., M.H., and F.H. designed research; C.M.M., S.J., G.F., F.D., B.V.L., and B.K. performed research; M.F.M. contributed new reagents/analytical tools; C.M.M., S.J., G.F., F.D., B.V.L., S.C.L.K., N.T., M.H., and F.H. analyzed data; and C.M.M. and F.H. wrote the paper.

The authors declare no conflict of interest.

This article is a PNAS Direct Submission. D.H. is a guest editor invited by the Editorial Board.

Published under the PNAS license.

Data deposition: The apo structures of PAS<sup>G4</sup> (PDB ID code 4CYR), PAS<sup>G7</sup> (PDB ID code 5AJ9), and PAS<sup>G9</sup> (PDB ID code 4CXX) and of PAS<sup>G4</sup> (PDB ID code 4CXS) and PAS<sup>G6</sup> (PDB ID code 4CYS) in complex with phenyl phosphonic acid and PAS<sup>G4</sup> in complex with 3-bromophenyl phenylphosphonate (PDB ID code 4CXU) have been deposited in the RCSB Protein Data Bank, [www.rcsb.org](http://www.rcsb.org).

<sup>1</sup>Present address: Michael Smith Laboratories, University of British Columbia, Vancouver, BC V6T 1Z4, Canada.

<sup>2</sup>Present address: Institut für Biochemie, Departement Biologie, ETH Zurich, 8093 Zürich, Switzerland.

<sup>3</sup>G.F. and F.D. contributed equally to this work.

<sup>4</sup>Present address: EaStCHEM School of Chemistry, University of Edinburgh, EH9 3FJ Edinburgh, United Kingdom.

<sup>5</sup>Present address: Institute for Evolution and Biodiversity, Westfälische Wilhelms-Universität, D48149 Münster, Germany.

<sup>6</sup>Present address: Synthetic and Systems Biology Unit, Institute of Biochemistry, Biological Research Centre of the Hungarian Academy of Sciences, 6726 Szeged, Hungary.

<sup>7</sup>To whom correspondence should be addressed. Email: [fh111@cam.ac.uk](mailto:fh111@cam.ac.uk).

This article contains supporting information online at [www.pnas.org/lookup/suppl/doi:10.1073/pnas.1607817115/-DCSupplemental](http://www.pnas.org/lookup/suppl/doi:10.1073/pnas.1607817115/-DCSupplemental).

Published online July 16, 2018.

example the conformation of the active site or the dynamics of loops in its vicinity, were concomitant with increases in catalytic efficiency (18, 27–30). Thus, gradual molecular tinkering, that is, the fine-tuning of existing interactions, is a successful strategy in adaptive evolution (31). Nonetheless, our understanding of the molecular mechanisms underlying functional transitions remains limited; alternative models may be required to elucidate the repurposing of enzymes with new or expanded catalytic repertoires.

Members of the alkaline phosphatase (AP) superfamily constitute paradigmatic examples to study how new functions—in particular with seemingly contrasting or even incompatible catalytic requirements—can emerge in one scaffold (32–36). The AP superfamily represents a large cluster of enzymes that catalyze a broad range of chemically distinct reactions, including the hydrolysis of sulfate, phosphate, and phosphonate monoesters or phosphodiester (37) (Fig. 1A). Notably, these substrates differ in their overall charge (singly or doubly negative) and the bond broken during catalysis (P–O vs. S–O). Furthermore, phosphate and sulfate monoesters undergo hydrolysis via a dissociative transition state (TS) (with little bond formation to the nucleophile and large charge buildup on the leaving group oxygen,  $O_{LG}$ ), while phosphonate monoesters and phosphodiester proceed through more associative TSs (characterized by greater

bonding to the nucleophile and less charge development at the  $O_{LG}$ ) (38–42) (Fig. 1B). Despite these differences, the AP superfamily exhibits extensive crosswise promiscuity, where the native activity of one member is the promiscuous activity of another, and vice versa. For example, besides sulfate esters, an arylsulfatase from *Pseudomonas aeruginosa* (PAS) (43–45) catalyzes the hydrolysis of phosphodiester and phosphonate and phosphate monoesters, with  $k_{cat}/K_m$  values ranging between  $10^{-2}$  and  $10^3 \text{ M}^{-1}\text{s}^{-1}$  (46–48), which represents a remarkable rate acceleration of  $10^8$ - to  $10^{18}$ -fold over the spontaneous hydrolysis in solution ( $k_{cat}/K_m/k_2$ ; *SI Appendix, Table S1*). Moreover, these promiscuous reactions exploit the same nucleophile, and likely the same (or at least a subset of the) catalytic residues as the native reaction (47, 49) (Fig. 1C and D). These observations suggest that enzyme promiscuity may have facilitated functional diversification within the AP superfamily. However, it remains unclear how its members can recognize such distinct substrates within a unique active site, and how evolution can repurpose enzyme functions by exploiting preexisting active-site features.

To address these issues, we created an evolutionary trajectory from the WT arylsulfatase (PAS<sup>WT</sup>) toward a weak promiscuous substrate, phosphonate monoester **2a**, over nine rounds of directed evolution. The resulting trajectory yielded a 100,000-fold

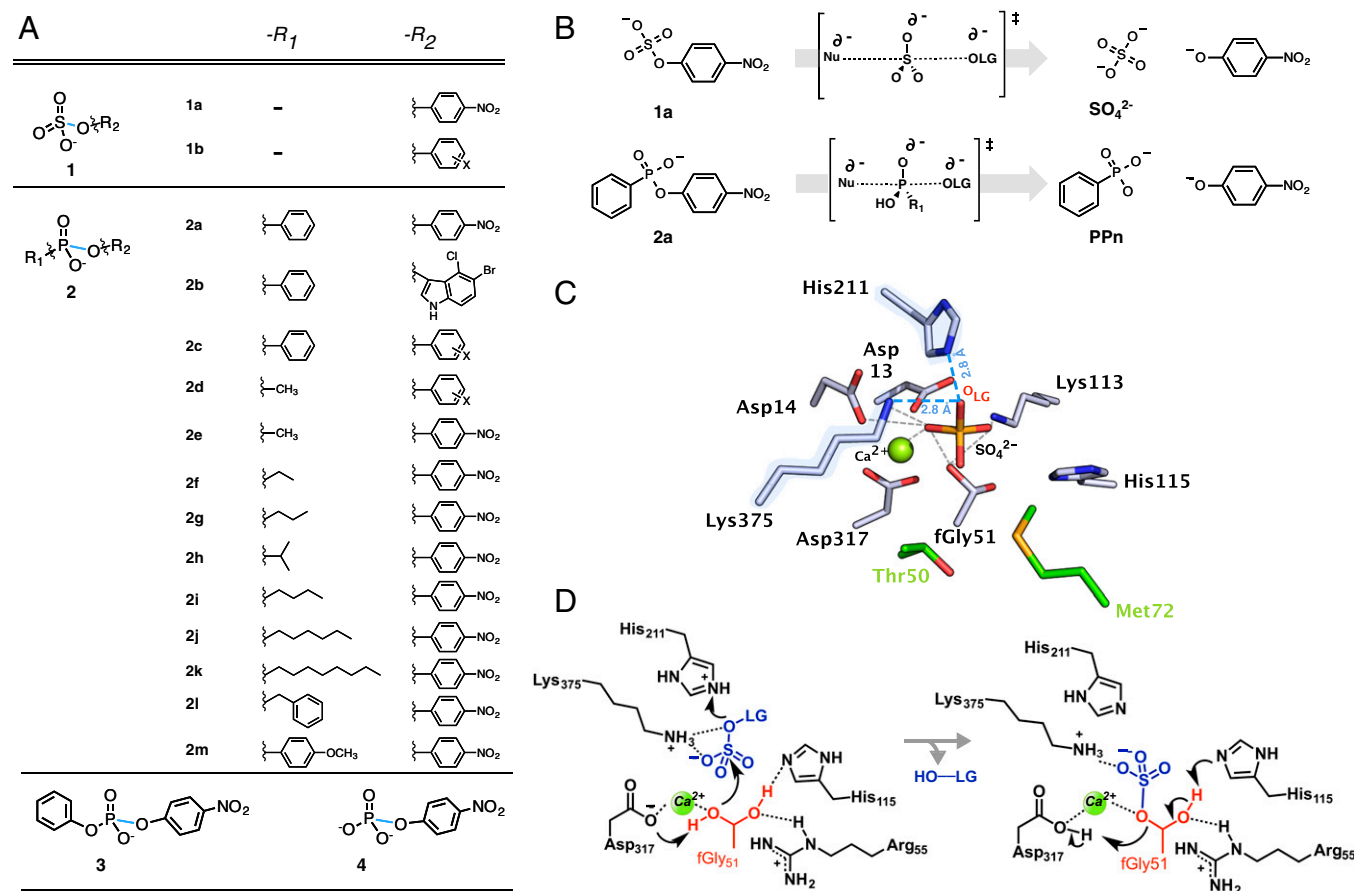


**Fig. 1.** PAS active site, mechanism, and substrates. (A) Substrates include sulfate monoesters **1**, phosphonate monoesters **2**, phosphate diesters **3**, and phosphate monoesters **4**, with various substituents **a–m** in position  $-R_1/-R_2$ . The scissile bond broken during hydrolysis is shown in blue. (B) The hydrolysis of sulfate **1a** originally catalyzed by PAS involves a dissociative TS, while the evolved target reaction, the hydrolysis of phosphonate monoester **2a**, proceeds through a more associative TS in solution. PPn stands for phenylphosphonic acid. (C) PAS<sup>WT</sup> active site with the cocrystallized ions sulfate- (orange sticks) and calcium- (green sphere) bound (43) and (D) a proposed mechanism for sulfate hydrolysis (43). (C and D) PAS<sup>WT</sup> possesses an fGly nucleophile, derived from a cysteine by posttranslational modification (44, 50). Nucleophilic attack by the Ca<sup>2+</sup>-coordinated fGly at the sulfur center leads to the departure of phenolate. A covalent fGly intermediate is formed and later cleaved by general base catalysis (H115). Assuming that the sulfate ion sits in the position resembling negatively charged substrates, the leaving group (LG) would depart in the direction where negative charge buildup on the LG oxygen ( $O_{LG}$  in red) requires stabilization. The residues contributing to catalysis are the cationic K375 and H211 (blue halo/dashes) that stabilize the LG, and D13, D14, D317, and fGly51 that coordinate the metal-ion and constitute possible hydrogen bonding donors/acceptors for the substrate (gray dashes) (49).

increase in phenylphosphonate hydrolase activity, one of the largest evolutionary increases observed, while paradoxically maintaining the originally broad specificity of PAS. Detailed kinetic, mechanistic, structural, and in silico analyses of several PAS intermediates and mutants revealed the mechanism of enzyme adaptation. These molecular insights provide an alternative model for functional transitions, which, in this case, occur via the creation of new Michaelis complexes, without major alteration of the existing catalytic core or the overall protein dynamics. Our results highlight how multiple catalytic functions can be supported by permissive active-site architectures and suggest features that may guide the search for promiscuous enzymes.

## Results

**Directed Evolution of an Arylsulfatase Toward Phenylphosphonate Hydrolysis.** The WT arylsulfatase (PAS<sup>WT</sup>) constituted the starting point for directed evolution (*SI Appendix, Methods and Fig. S1*). The mechanism of sulfate esters hydrolysis relies on a sequence of displacements, involving initial nucleophilic attack at the sulfur center using a Ca<sup>2+</sup>-activated formylglycine (fGly) nucleophile derived from a posttranslationally modified cysteine (44, 50) (Fig. 1D). Efficient TS stabilization is achieved by the cationic residues K375 and H211 that offset the negative charge buildup on the leaving group oxygen (O<sub>LG</sub>) as the TS is approached (43), leading to a  $k_{\text{cat}}/K_m$  of  $10^7 \text{ M}^{-1}\cdot\text{s}^{-1}$  (47). The promiscuous phosphonate **2a** was chosen as a target substrate as it is characterized by a very low rate of hydrolysis in PAS<sup>WT</sup> ( $k_{\text{cat}}/K_m = 1.47 \times 10^{-2} \text{ M}^{-1}\cdot\text{s}^{-1}$ ) (Table 1). Indeed, the cleavage of phosphonates **2a-b** by PAS<sup>WT</sup> is so slow that it could not be distinguished from their hydrolysis by endogenous *Escherichia coli* proteins on agar plate colony screening or in cell lysate assays (*SI Appendix, Fig. S2A*). Thus, initial attempts to isolate variants with increased phenylphosphonate hydrolase activity from PAS<sup>WT</sup> remained unsuccessful, despite screening well above 10,000 colonies. In an alternative approach to break this deadlock, three rounds of evolution were performed under neutral drift conditions (51, 52), in which mutations were accumulated slowly (genetic drift), while purging the clones that lost the ability to degrade the native sulfate **1** substrate. This typically leads to an enrichment of functional mutants at each round. To this end, libraries of mutagenized PAS were generated by error-prone PCR and screened for activity toward the original sulfate **1a**. All variants that possessed more than 5% of the sulfatase activity of PAS<sup>WT</sup> in crude lysate were pooled and used as templates for the next round of mutagenesis (*SI Appendix, Fig. S2B and Table S2*). After three rounds of neutral drift ( $L_{1-3}$ ), 37% of variants (183 out

of 445 variants) retained sulfatase activity above the threshold and bore, on average, approximately five amino acid mutations.

At this stage, library  $L_4$  was subjected to screening in a two-step assay (*SI Appendix, Fig. S1*) to isolate variants with enhanced phenylphosphonate hydrolase activity, thus moving from purifying to adaptive selection. Library  $L_4$  yielded ~100 positive variants with enhanced promiscuous phenylphosphonate hydrolase activity, suggesting that the neutral drift prelude successfully increased the chance of subsequent adaptive evolution via accumulation of multiple mutations. The most improved clone PAS<sup>G4</sup> possesses six mutations, of which two, T50A and E461G, are largely responsible for the increase in phosphonate hydrolase activity (*SI Appendix, Fig. S2 C and D*). The catalytic efficiency of PAS<sup>G4</sup> for the hydrolysis of phosphonate **2a** was enhanced by ~2,800-fold, compared with PAS<sup>WT</sup> (Table 1). The following rounds 5–9 (libraries  $L_{5-9}$ ) gave rise to mutants with a gradual increase in phosphonate hydrolase activity through a stepwise addition of mutations (*SI Appendix, Fig. S3 and Table S3*). The ultimate variant PAS<sup>G9</sup> bears nine mutations and exhibits a 190-fold improvement in phosphonate **2a** hydrolysis in lysate over PAS<sup>WT</sup>, corresponding to a  $10^5$ -fold increase in  $k_{\text{cat}}/K_m$  ( $k_{\text{cat}}/K_m = 1.64 \times 10^3 \text{ M}^{-1}\cdot\text{s}^{-1}$ ) (Table 1). Further attempts to significantly enhance PAS<sup>G9</sup> activity with additional substitutions (round 10) were unsuccessful. The first improvement in phenylphosphonate hydrolase activity (in PAS<sup>G4</sup>) can be largely apportioned to a decrease in  $K_m$  (175-fold, from 10 mM to 59  $\mu\text{M}$ ) and, to a lesser extent, to an increase in  $k_{\text{cat}}$  (15-fold). The second phase of the respecialization (rounds 4–9) involves a further 46-fold increase in  $k_{\text{cat}}$  (Table 1). Although  $K_m$  can be lower or equal to the dissociation constant ( $K_d$ ) in the two-step mechanism of PAS [in absence of limiting diffusion (53)],  $K_m$  represents the upper limit of the binding affinity of the Michaelis complex (*SI Appendix, Scheme S1*). Therefore, the observed decrease in  $K_m$  (150-fold) early in the trajectory suggests a necessary adaptation of binding, as the first accessible conduit for respecialization.

**Functional Trade-Offs Among Four Hydrolytic Reactions Reveal Substrate-Dependent Evolutionary Constraints.** To quantify the impact of the evolution toward phosphonate **2a** on the specificity profile of PAS<sup>WT</sup> and its variants, we measured the kinetic parameters for three other chemically distinct substrates: sulfate **1a**, phosphodiester **3**, and phosphate monoester **4** (Fig. 2 and *SI Appendix, Table S4*). The hydrolysis of these substrates by PAS was not selected for or against in our trajectory; thus, it never was under direct evolutionary pressure. In PAS<sup>G9</sup>, the  $10^5$ -fold increase in phosphonate **2a** hydrolysis was accompanied by a 400-fold decrease in native sulfate **1a** hydrolysis, mostly as a result of

**Table 1. Kinetic parameters of PAS<sup>WT</sup> and mutants at 25 °C, pH 8.0**

PAS	Mutations	Phosphonate <b>2a</b>			Sulfate <b>1a</b> *			
		$k_{\text{cat}}, \text{s}^{-1}$	$K_m, \mu\text{M}$	$k_{\text{cat}}/K_m, \text{M}^{-1}\cdot\text{s}^{-1}$	$k_{\text{cat}}, \text{s}^{-1}$	$K_m, \mu\text{M}$	$k_{\text{cat}}/K_m, \text{M}^{-1}\cdot\text{s}^{-1}$	Spe <sup>†</sup>
WT		$1.5 \times 10^{-4}$	10,400	0.015	15.9	1	$2.30 \times 10^7$	$10^{-10}$
G4	T50A, E523D, G337D, E461G, A22T, S134A	$2.5 \times 10^{-3}$	59	42	‡	‡	$2.56 \times 10^6$	$10^{-5}$
G5	PAS <sup>G4</sup> + M72V, E449A	$2.9 \times 10^{-1}$	150	1,930	3.0	16	$1.89 \times 10^5$	$10^{-2}$
G6	T50A, E523D, G337D, E461G, M72V, R352S	$1.1 \times 10^{-1}$	140	786	1.5	14	$1.03 \times 10^5$	$10^{-3}$
G7	PAS <sup>G6</sup> + I69L	$3.0 \times 10^{-1}$	106	2,830	12.6	61	$2.06 \times 10^5$	$10^{-2}$
G9	PAS <sup>G7</sup> + A48T, V535E	$1.1 \times 10^{-1}$	70	1,640	6.1	103	$5.93 \times 10^4$	$10^{-3}$
T50A	T50A	$3.6 \times 10^{-4}$	28	13	‡	‡	$4.13 \times 10^6$	$10^{-6}$
M72V	M72V	$3.0 \times 10^{-5}$	44	0.7	8.8	106	$8.32 \times 10^4$	$10^{-6}$
T50A/M72V	T50A, M72V	$9.1 \times 10^{-2}$	97	939	13.8	81	$1.71 \times 10^5$	$10^{-3}$

All kinetics typically performed in triplicate for >24 data points, in 100 mM Tris-HCl and 0.5 M NaCl, pH 8.0, at 25 °C. The means and SEs of all kinetic parameters originate from a fit to Eqs. E1–E3 and are shown in *SI Appendix, Table S4*.

\*Substrate inhibition by sulfate **1a** arose from round 4 onward ( $K_i$  are presented in *SI Appendix, Table S4*).

<sup>†</sup>Specificity is the ratio of the  $k_{\text{cat}}/K_m$  values for phosphonate **2a** vs. sulfate **1a** hydrolase activity.

<sup>‡</sup>Nonmeasurable due to high substrate inhibition, preventing an accurate determination of individual kinetic parameters.



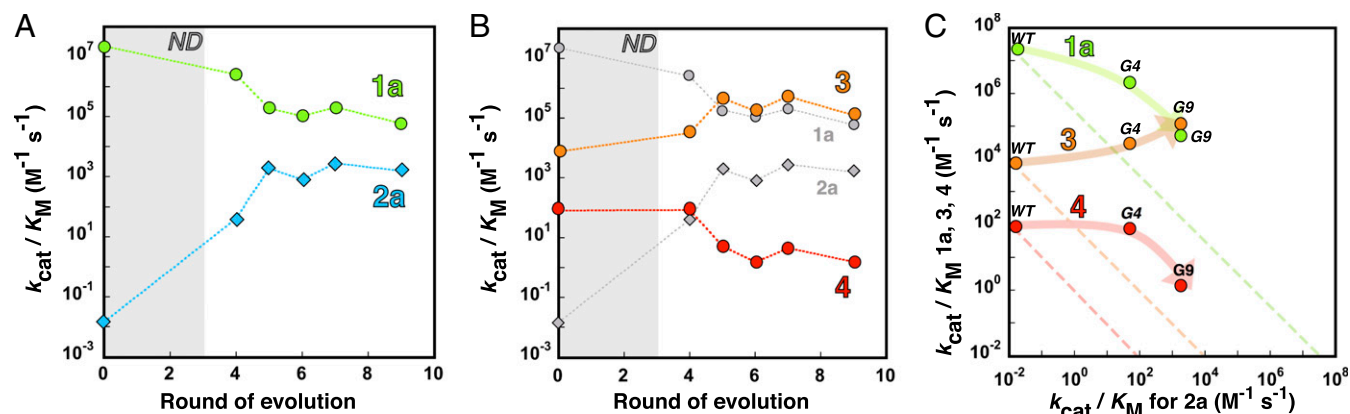


**Fig. 2.** Evolutionary trajectories of PAS for native and promiscuous reactions. Evolution of the Michaelis–Menten parameters ( $k_{\text{cat}}/K_{\text{M}}$ ) for (A) the evolved phosphonate hydrolase (2a, blue) and the native sulfatase activities (1a, green). (B) Changes in  $k_{\text{cat}}/K_{\text{M}}$  values for the hydrolysis of the promiscuous phosphate diester 3 (orange) and phosphate monoester 4 (red). Data for 1a and 2a are shown in gray for comparison. (C) Activity trade-offs between sulfatase (1a, green), phosphodiesterase (3, orange), and phosphatase (4, red) activities vs. phosphonate 2a activity. For comparison, linear activity trade-offs, that is, when the gain of the new function equals the loss of the old one, are depicted as dashed lines.  $k_{\text{cat}}/K_{\text{M}}$  are plotted for each activity on a logarithmic scale. ND stands for neutral drift (rounds 1–4) where no intermediate was isolated. Measurements were typically performed in triplicate for  $n > 24$  data points. Data and SEs are listed in *SI Appendix, Table S4*.

a strong increase in  $K_{\text{M}}$  (147-fold), while  $k_{\text{cat}}$  is only halved. Overall, PAS<sup>G9</sup> exhibits a  $4 \times 10^7$ -fold change in specificity between phenylphosphonate and sulfate monoesters compared with PAS<sup>WT</sup> (Fig. 2A and Table 1), with an asymmetric effect on the two activities: The activity increase toward phosphonate 2a is 250-fold larger than the decrease in sulfatase activity (1a). The promiscuous phosphodiesterase activity increased along with the phosphonate hydrolase activity, but to a much smaller degree (30-fold increase in  $k_{\text{cat}}/K_{\text{M}}$ ) (Fig. 2B). By contrast, the phosphate monoesterase activity decreased by 53-fold, following a trend similar to the cognate sulfatase activity (1a). Covariation of phosphonate 2a hydrolase/phosphodiesterase 3 and sulfatase 1a/phosphatase 4 activities can be assigned to (i) a similar shape and/or charge (2a and 3 each bear two bulky phenyl rings; 1a and 4 are smaller and almost isosteric) or (ii) the comparable nature of the TSs through which they proceed (the first pair being more associative, the second dissociative). Overall, the adaptation of PAS toward improved phosphonate 2a hydrolysis results in weak trade-offs, where the substantial improvement of one function is obtained at the cost of a moderate loss in all of the other promiscuous activities (Fig. 2C). Consistent with previous observations (17, 18, 25), the sequence of purifying and adaptive evolution has brought about an enzyme with features of a “generalist” compared with PAS<sup>WT</sup>, in the sense that the four activities are covered in a narrower range (with the  $k_{\text{cat}}/K_{\text{M}}$  range decreasing from  $10^9$  to  $10^4$ ). Furthermore, the difference in second-order rate enhancement between sulfate 1a and phosphonate 2a has been reduced from 10 orders of magnitude in PAS<sup>WT</sup> to only three in PAS<sup>G9</sup> [ $(k_{\text{cat}}/K_{\text{M}})_{k_2} = 7.5 \times 10^{13}$ ; *SI Appendix, Table S1B*]. These results suggest that the chemical machinery of PAS<sup>WT</sup> is intrinsically reactive and promiscuous (even with respect to difficult reactions), a feature that appears to have been further enhanced by evolution. Evolution for increased phosphonate hydrolysis paradoxically achieved higher specificity for phosphonate 2a, while it largely relaxed the selectivity for all other substrates.

**Mutations T50A and M72V Are Key to Converting PAS<sup>WT</sup> into a Proficient Phosphonate Hydrolase.** Throughout the directed evolution, none of the residues belonging to the catalytic core (fGly51, K375, H115, H211, D317, and Ca<sup>2+</sup>) (47, 54) were substituted. Out of nine mutations accumulated over nine rounds, two (T50A and M72V) are located in the active-site cleft in the close vicinity of the fGly nucleophile (fGly51, Fig. 3). To determine the effects of these two mutations, single and double mutants PAS<sup>T50A</sup>, PAS<sup>M72V</sup>, and PAS<sup>T50A/M72V</sup> were generated

on the PAS<sup>WT</sup> background, purified, and characterized. T50A provides an ~880-fold increase in phosphonate hydrolase activity (against 2a), which accounts for most of the improvement between PAS<sup>WT</sup> and PAS<sup>G4</sup>, while M72V contributes to the extra ~46-fold increase seen in PAS<sup>G5</sup> (Table 1). The double mutant exhibits a 63,000-fold increase for phosphonate 2a, which is only ~1.8-fold less than PAS<sup>G9</sup>, indicating that T50A and M72V are mainly responsible for the improvement in phosphonate hydrolase activity during evolution. These mutations are additive with regard to their ability to increase phosphonate hydrolase 2a activity (*SI Appendix, Fig. S4*). The decrease in sulfatase 1a activity is also largely mediated by these two mutations: the double mutant exhibiting a 130-fold decrease, making it only three times more active than PAS<sup>G9</sup>. In contrast to additive effects, we observe epistatic synergistic effects on sulfate hydrolysis: T50A and M72V alone reduce this activity by 6- and 280-fold, respectively, but their combined effect (an observed 130-fold decrease) falls short of the 1,680-fold effect expected from full additivity. Mutation E461G was also assayed in combination with T50A and increases the phosphonate hydrolase activity by approximately ninefold (PAS<sup>T50A/E461G</sup>, *SI Appendix, Fig. S2C*). Mutations I69L and A48T do not contribute significantly to the increase in phosphonate hydrolase activity in the later stages of the trajectory, despite their close proximity to T50A and M72V. Four mutations (R352S, G337D, E523D, and V535E) are positioned at the surface of the protein, consistent with either functional neutrality and/or a possible improvement of the stability of the protein (folding, solubility, and expression).

**T50A and M72V Reshape the Active Site, Improving Enzyme–Substrate Complementarity.** To understand the molecular mechanisms responsible for the altered specificity, PAS<sup>WT</sup> together with PAS<sup>G4</sup>, PAS<sup>G6</sup>, PAS<sup>G7</sup>, and PAS<sup>G9</sup> were crystallized in their apo form or complexed with ligands, and their structures resolved by X-ray crystallography with ~1.7- to 2.3-Å resolution (Fig. 3 and *SI Appendix, Fig. S5 and Table S5*). Rather than the profound rearrangements that may be expected for functional changes of this magnitude, the backbone of the protein coincides for PAS<sup>WT</sup> and all of the evolved species (rmsd of PAS<sup>WT</sup> structure with all mutants is 0.13–0.21 Å). Moreover, the position of the catalytic residues previously identified as such (fGly51, K375, H115, H211, and D317) also remains unchanged (*SI Appendix, Fig. S6*), suggesting that this particular organization is sufficient to maintain the hydrolysis of all classes of substrates (Fig. 3A). However, the active site appears reshaped by T50A and M72V (Fig. 3B–E), two residues that were not previously identified as

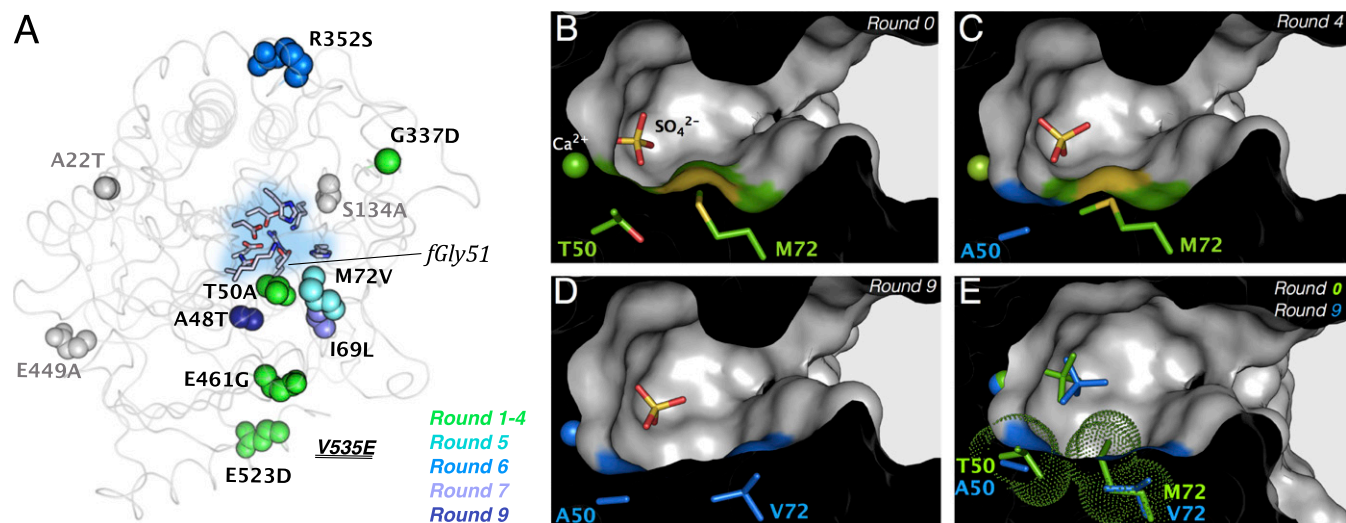


**Fig. 3.** Mutations T50A and M72V reshaped the active site of PAS. (A) Backbone diagram of PAS<sup>WT</sup> (PDB ID code 1hdh) with mutations accumulated during directed evolution depicted as spheres. Mutations are colored according to their occurrence in the trajectory; reversions back to WT are in gray. The catalytic residues are depicted as sticks and a blue background highlights the active-site pocket. V535E (PDB ID code 4cyr) is not shown, as no electron density was observed for residues 527–536 in the PAS<sup>WT</sup> structure. (B–E) Cut-through representations of the active site of (B) PAS<sup>WT</sup> (PDB ID code 1hdh), (C) PAS<sup>G4</sup> (PDB ID code 4cyr), and (D) PAS<sup>G9</sup> (PDB ID code 4cxk), highlighting evolutionary reshaping. Positions T50 and M72 are depicted as sticks and Ca<sup>2+</sup> as a sphere and are colored in green before mutation or blue after (res. A50, V72). (E) Overlay of PAS<sup>WT</sup> and PAS<sup>G9</sup> (van der Waals radii rendered as dots), emphasizing changes in active-site volumes during evolution.

relevant to catalysis (49, 54). First, T50A enlarges the active site near the nucleophile, fGly51 (Fig. 3C). Then, M72V further opens the active-site cavity opposite A50 (Fig. 3D). Overall, PAS<sup>G9</sup> possesses a ~1.5-fold larger active-site volume compared with PAS<sup>WT</sup> (~1,900 Å<sup>3</sup> vs. ~2,900 Å<sup>3</sup>; *SI Appendix, Fig. S7*). Taken together with the 370-fold lower  $K_m$  for PAS<sup>T50A</sup> compared with PAS<sup>WT</sup>, these results are consistent with a widening of this side pocket to satisfy the increased space requirement for accommodation of the bulky phenyl substituent of phosphonate **2a**, which is absent in sulfate **1a**.

**Size and Shape Constrain Substrate Access to the Active Site and Limit Catalytic Promiscuity in PAS.** To address how steric properties of the substrate affect binding and specificity along the evolutionary trajectory, a broad range of alkyl- and phenyl phosphonates varying the nonreactive side-chain R<sub>1</sub> (**2e–m**) was synthesized (Fig. 1A) and the relationship between substrate structure and  $k_{cat}/K_m$  measured for all PAS mutants (Fig. 4 and *SI Appendix, Table S6*).  $k_{cat}/K_m$  values of PAS<sup>WT</sup> for most of the substituted phosphonates range between 10<sup>2</sup> and 10<sup>5</sup> M<sup>-1</sup>·s<sup>-1</sup> (Fig. 4), demonstrating that PAS<sup>WT</sup> can act as a rather efficient phosphonate hydrolase, when phosphonate substrates bear a small and/or conformationally flexible side chain. By contrast, bulky substituents such as phenyl, methoxyphenyl, and isopropyl result in greatly reduced catalytic efficiencies: their  $k_{cat}/K_m$  values ( $\leq 10^{-2}$  M<sup>-1</sup>·s<sup>-1</sup>) are seven orders of magnitude lower than for the smallest phosphonate **2e**, suggesting a substantial penalty from steric hindrance in PAS<sup>WT</sup>. PAS<sup>WT</sup> exhibits a high phosphodiesterase activity ( $k_{cat}/K_m = 4.3 \times 10^3$  M<sup>-1</sup>·s<sup>-1</sup>), despite the fact that diester **3** contains two phenyl substituents (making it sterically similar to phosphonate **2a**). The flexibility afforded by the insertion of an oxygen atom between reaction center and substituent in phosphonate **2a** (P–O–C vs. P–C) is likely causing these differences. The significant increase in phenyl-phosphonate **2a** hydrolysis during the evolution (10<sup>5</sup>-fold) is correlated to an increase in catalytic efficiency for most phosphonates, albeit to a much lesser extent (10- to 22-fold increase in  $k_{cat}/K_m$ ). However, hydrolysis of the methoxyphenyl-substituted phosphonate **2m** (closely resembling **2a**) also increases by 660-fold. Methyl phosphonate **2e** (sterically more similar to sulfate **1a**) is the only substrate with a decreased  $k_{cat}/K_m$  (17-fold). These results suggest that during

the laboratory evolution PAS mainly overcame the effect of a bulky, nonalkylated substituent (such as phenyl in phosphonate **2a**) and that steric (or geometrical) complementarity is limiting promiscuity, specifically preventing phosphonate **2a** from being turned over efficiently. We thus hypothesized that the evolved variant PAS<sup>G9</sup> enables binding of phosphonate **2a** in a distinct, more favorable orientation compared with PAS<sup>WT</sup>. By contrast, the enlarged active site likely results in a higher degree of freedom for sulfate **1a** and methyl phosphonate **2e** binding, consistent with a 150- and 6-fold increase in  $K_m$ , respectively, between PAS<sup>WT</sup> and PAS<sup>G9</sup>.

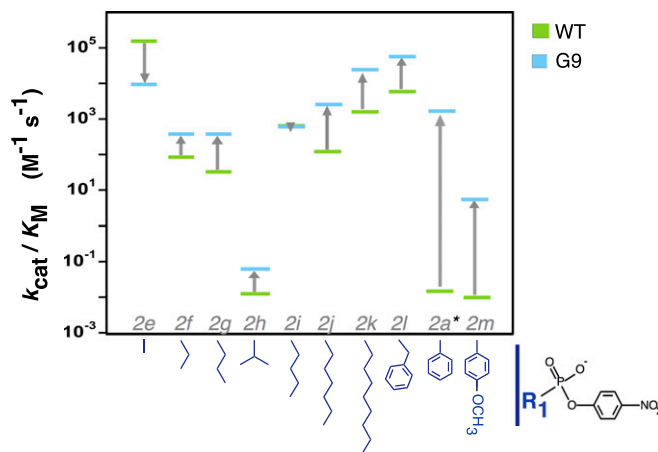


**Fig. 4.** Nonreacting substituents  $-R_1$  of phosphonate monoesters determine promiscuous hydrolysis rates throughout PAS evolution. Relative  $k_{cat}/K_m$  enhancements (gray arrows) between PAS<sup>WT</sup> (green lines) and PAS<sup>G9</sup> (cyan lines) for a series of substituted phosphonates **2** ( $-R_1 = 2a$ : phenyl, **2e**: methyl, **2f**: ethyl, **2g**: propyl, **2h**: isopropyl, **2i**: butyl, **2j**: hexyl, **2k**: octyl, **2l**: benzyl, **2m**: methoxyphenyl; full structures in Fig. 1). The biggest effect (\*) is observed on the acceptance of phosphonate **2a** with a large phenyl substituent, resulting in a 10<sup>5</sup>-fold increase in  $k_{cat}/K_m$  for this substrate. Measurements were typically performed in triplicate for  $n > 24$  data points. Data and SE are presented in *SI Appendix, Table S6*.

**Changes in Charge Offset in the TS During Evolution.** Linear free-energy relationships (Brønsted plots) were measured to investigate the charge changes as the TS is approached from the ground state (GS) (41) (Fig. 5 and *SI Appendix*, Fig. S8 and Table S7). The slope of this plot,  $\beta_{LG}$ , correlates rates for substrates with varying leaving group to the leaving group  $pK_a$  ( $pK_a^{LG}$ ) and reports on the effective charge change “seen” at the site of bond cleavage (in this case, on the  $O_{LG}$ ) as the TS is approached. The stabilization of the charge developing in the TS must be a key task for an efficient enzyme: If the  $\beta_{LG}$  changes between WT and mutants, then changes in the extent of charge stabilization reflect the impact of evolution on the catalytic step. As  $k_{cat}/K_m$  encompasses the rate of all reaction steps up to, and including, the first irreversible step (in this case phenolate departure described by  $k_2$ ; *SI Appendix*, Scheme S1), possible explanations that involve effects on breakdown of the covalent intermediate ( $k_3$ ) or other subsequent steps can be ruled out. Also, the reaction rates are well below the diffusion limit and insensitive to viscogen in PAS (53), discounting that a non-chemical step associated with diffusion became progressively rate-limiting. Finally, altered  $\beta_{LG}$  values can be explained by a change in the nature of the TS (55, 56). However, in the AP superfamily previous evidence suggests that TSs are hard to change and that enzymatic catalysis stabilizes TSs of similar nature to the reaction in solution (38, 57, 58). Kinetic isotope effects measured for PAS show only minor changes and support this view (53).

The Brønsted slope for the hydrolysis of phenyl phosphonates **2c** is steepest in  $PAS^{WT}$  ( $\beta_{LG} = -1.08$ ), and significantly larger than that for the uncatalyzed reaction [ $\beta_{LG}^{solution} = -0.69$  with aryl methyl phosphonates (55)] (Fig. 5A). This value could be rationalized by a departure of the substrate leaving group oxygen  $O_{LG}$  in a hydrophobic environment, where hydrogen bonding is weaker or entirely excluded, compared with the situation in water. As evolution proceeds, the slope gradually becomes shallower in  $PAS^{T50A}$ ,  $PAS^{G4}$ , and  $PAS^{G9}$  ( $\beta_{LG} = -0.42$ ). This dramatic change in  $\beta_{LG}$  can be ascribed to mutation T50A ( $\Delta\beta_{LG}^{WT-T50A} = 0.58$ ) and accompanies a large decrease in  $K_m$  in this single mutant (370-fold). However, additional mutations, including M72V, alter the slope only slightly ( $\Delta\beta_{LG}^{G4-G9} = 0.08$ ). Paradoxically, the same linear free-energy relationship (LFER) analysis using the sterically less demanding methyl

phosphonates **2d** shows that evolution does not alter the  $\beta_{LG}$  in this case ( $\beta_{LG} \sim -0.59$ ) (Fig. 5B). This observation suggests that, unlike for phenylphosphonate **2a**, the specific catalytic features of leaving group stabilization in **2d** are not affected by the evolution: Without steric hindrance to remedy, no repositioning of **2d** in the active site takes place.

As the efficiency of the original sulfatase activity decreases during evolution, the effective charge change on  $O_{LG}$  of sulfate **1b** exhibits a behavior opposite to that of phosphonate **2a**: The  $\beta_{LG}$  for sulfates **1b** increases from  $-0.34$  for  $PAS^{WT}$  to  $-0.79$  for  $PAS^{G9}$ , indicating a loss of leaving group stabilization (Fig. 5C). The increased  $\beta_{LG}^{PAS^{G9}}$  for the sulfatase reaction does not reach the corresponding value in solution ( $\beta_{LG}^{solution} = -1.81 \pm 0.09$ ) (59): As  $PAS^{G9}$  is still a “good” sulfatase ( $k_{cat}/K_m = 5.9 \times 10^4 \text{ M}^{-1}\text{s}^{-1}$ ) some leaving group stabilization must remain. Mutation T50A in  $PAS^{G4}$  has virtually no effect on the  $\beta_{LG}$  for the sulfatase activity ( $\Delta\beta_{LG}^{WT-G4} = 0.01$ ), while  $PAS^{G9}$  shows a significant increase in  $\beta_{LG}$  ( $\Delta\beta_{LG}^{G4-G9} = 0.44$ ), suggesting that M72V has largely compromised the charge offset at the  $O_{LG}$  in the TS. Similar to the case of phosphonate **2b**, the increase in  $\beta_{LG}$  is correlated to changes in  $K_m$  (150-fold increase from  $PAS^{WT}$  to  $PAS^{G9}$ ).

The strong impairment of leaving group stabilization observed for sulfates **1b** resembles the knock-out of a leaving group-stabilizing residue: mutation K375A in  $PAS^{WT}$  causes a large drop in  $\beta_{LG}$  ( $\Delta\beta_{LG}^{WT-K375A} = 0.63$ , Fig. 5C), akin to the trend observed in  $PAS^{G9}$ . Conversely the shallower  $\beta_{LG}$  for phosphonate **2a** is likely associated with an increasingly efficient quenching of the negative TS charge developing on the  $O_{LG}$ , which decreases the sensitivity of the reaction to the nature of the leaving group, without influencing the degree of bond cleavage at the TS. As the position of the catalytic residues, in particular K375 and H211, is not significantly altered by evolution (*SI Appendix*, Fig. S6), our findings suggest the creation of a new Michaelis complex, where the substrate GS is reoriented with respect to the catalytic machinery. Consequently, TS interactions are improved for phosphonate **2a** and compromised for sulfate **1a**.

**Substrate Repositioning During Evolution from  $PAS^{WT}$  to  $PAS^{G9}$ .** To test the hypothesis of a repositioning of GSs (suggested by changes in  $K_m$ ) and TSs (suggested by changes in  $\beta_{LG}$ ) with respect to the

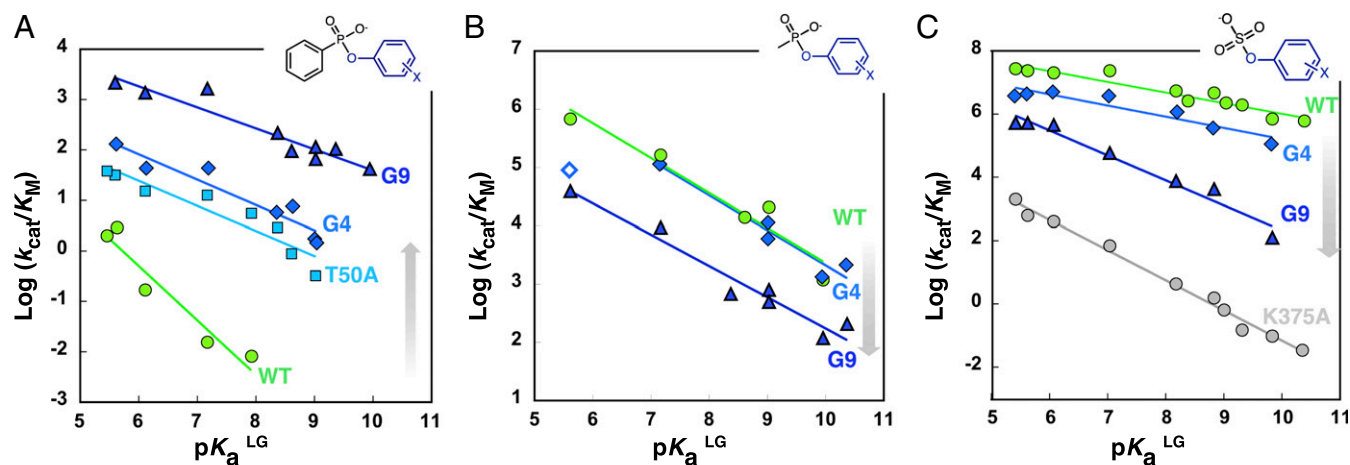


**Fig. 5.** Evolution alters the charge “seen” by the leaving group oxygen at the TS of promiscuous phosphonates **2c** and **2d** and native sulfates **1b**. Linear free-energy analyses for the (A) hydrolysis of phosphonates **2b** gives  $\beta_{LG}$  slopes of  $-1.08 \pm 0.17$  ( $PAS^{WT}$ , green circles),  $-0.50 \pm 0.07$  ( $PAS^{T50A}$ , cyan squares),  $-0.50 \pm 0.07$  ( $PAS^{G4}$ , blue diamonds), and  $-0.42 \pm 0.05$  ( $PAS^{G9}$ , dark blue triangles) that become increasingly shallow throughout evolution. The gray arrow indicates the evolutionary transition from  $PAS^{WT}$  to  $PAS^{G9}$ . (B) By contrast, the  $\beta_{LG}$  for phosphonates **2c** (bearing a methyl instead of phenyl substituent as the non-reactive group) is not significantly altered by evolution ( $\beta_{LG}$  values of  $-0.60 \pm 0.09$  for  $PAS^{WT}$  and  $PAS^{G4}$ ,  $-0.54 \pm 0.05$  for  $PAS^{G9}$ ). The 2-fluoro-4-nitro substituted phosphonate **2c** (open symbol) was omitted from the correlation due to its consistent deviation from linearity for  $PAS^{G4}$  only (despite triplicate measurement). (C) The corresponding correlations for sulfate monoesters **1b** provide  $\beta_{LG}$  values of  $-0.34 \pm 0.03$  ( $PAS^{WT}$ ),  $-0.35 \pm 0.06$  ( $PAS^{G4}$ ), and  $-0.79 \pm 0.07$  ( $PAS^{G9}$ ). Residue K375, involved in LG stabilization, was mutated to alanine ( $PAS^{K375A}$ , gray circles); this causes a steep relationship ( $\beta_{LG} = -0.95 \pm 0.03$ ) with the  $pK_a^{LG}$ , sign of compromised assistance to the departing phenolate. Data and SE are presented in *SI Appendix*, Table S7.



key catalytic residues, we initially attempted to introduce TS analogs (e.g., magnesium fluoride or vanadate), a reaction product (phenyl phosphonic acid, *PPn*), and a slowly hydrolyzing phosphonate (**2c** with a 3-bromophenol leaving group, *3Br*) into the active site of PAS<sup>WT</sup> and its mutants. However, soaking of TS analogs was unsuccessful and non- or slowly reactive substrates only led to ligand binding in nonproductive orientations (*SI Appendix*, Fig. S5). Therefore, molecular dynamics (MD) simulations were performed to illustrate the GS binding of phosphonate **2a** and sulfate **1a** in PAS<sup>WT</sup>, PAS<sup>G9</sup>, and mutants T50A, M72V, and T50A/M72V (Fig. 6). Each variant was equilibrated for a total of 200 ns over four replicates with different initial velocities (i.e., four independent 50-ns simulations for each system), leading to a total of 1.2  $\mu$ s of cumulative time for all of the variants, and convergence was reached in all simulations (*SI Appendix*, Fig. S9 and Tables S11–S15).

The simulations of the PAS<sup>WT</sup>–phosphonate **2a** complex corroborate the hypothesis that the monitored distances between the substrate and the catalytic residues directly contacting it in the GS were significantly shortened as evolution proceeds (Fig. 6 and *SI Appendix*, Table S8). From PAS<sup>WT</sup> to PAS<sup>G9</sup>, phosphonate **2a** is comparatively shifted by  $\sim 0.2$  Å closer to the leaving group stabilizing residue K375 (K375...O<sub>LG</sub>, from 3.71 to 3.49 Å),  $\sim 0.6$  Å closer to the nucleophile (O<sub>NUC</sub>...P, distance between nucleophile and phosphorus, from 3.79 to 3.21 Å), and  $\sim 1.1$  Å closer to the calcium ion (Ca<sup>2+</sup>...O = P, distance between the calcium and the closest nonbridging oxygen, from 3.82 to 2.72 Å; Fig. 6 *A* and *C*). Additionally, the compromised in-line positioning observed in PAS<sup>WT</sup> between the fGly nucleophile and the P center has been optimized by evolution (angle O<sub>NUC</sub>...P...O<sub>LG</sub>  $\sim 153.2^\circ$  in PAS<sup>WT</sup> vs.  $\sim 165^\circ$  in PAS<sup>G9</sup>; *SI Appendix*, Table S8). Finally, the calculated electrostatic interaction free energy ( $\Delta G_{\text{ELEC}}$ ) between the phosphonate **2a** and the protein increases from PAS<sup>WT</sup> to PAS<sup>G9</sup>, suggesting that a more energetically favored Michaelis complex was formed in PAS<sup>G9</sup> (*SI Appendix*, Fig. S10).

As all catalytic residues retained their original position in the WT and mutant structures (consistent with crystallographic evidence; Fig. 6), changes in angles and distances can be ascribed to a repositioning of the substrate's GS with respect to key catalytic residues (as no restricted dynamic constraints were applied in the simulation). Reaffirming the kinetic and structural evidence mentioned above, these results illustrate the existence of a steric conflict in PAS<sup>WT</sup>, between the phenyl ring (R<sub>2</sub>) of phosphonate **2a** and the side chain of T50, preventing the formation of an efficient Michaelis complex with **2a** (Fig. 6*A*). Evolution resolved this conflict in PAS<sup>G9</sup> by repositioning phosphonate **2a** closer to the catalytic center for enhanced catalysis. Despite being a GS effect, a similar trend must be presumed in the TS: The observed reduction in bond distance between K375 and the O<sub>LG</sub> in the MD suggests better offset of the developing negative charge in the TS, consistent with the shallower  $\beta_{\text{LG}}$  slope observed in the LFER (Fig. 4).

In the case of sulfate **1a**, the origin of the decrease in catalysis is less evident in MD simulations: The changes in distance and positioning of the cognate substrate appear marginal (Fig. 6 *B* and *D*). As the MD protocol minimizes energy terms, the observation that sulfate **1a** reaches a similar GS orientation in the mutant suggests that in the absence of a steric clash between the GS and the catalytic core, a Michaelis complex formation, similar to the “nearly perfect” WT one, remains allowed in PAS<sup>G9</sup> (Fig. 6 *B* and *D* and *SI Appendix*, Fig. S10). However, the sulfate ion that cocrystallized in PAS<sup>G4-G9</sup>, and which can be taken as a proxy for the sulfate moiety of **1a**, is reoriented in the active site: Measured from its central sulfur, the sulfate ion is displaced by 0.8–1 Å, accompanied by a  $\sim 41$ – $80^\circ$  flip compared with its position in PAS<sup>WT</sup> (*SI Appendix*, Fig. S11). This alternative orientation suggests a weakening of the interactions to the sulfate moiety, upon loss of contacts with the metal ion and D13/D14.

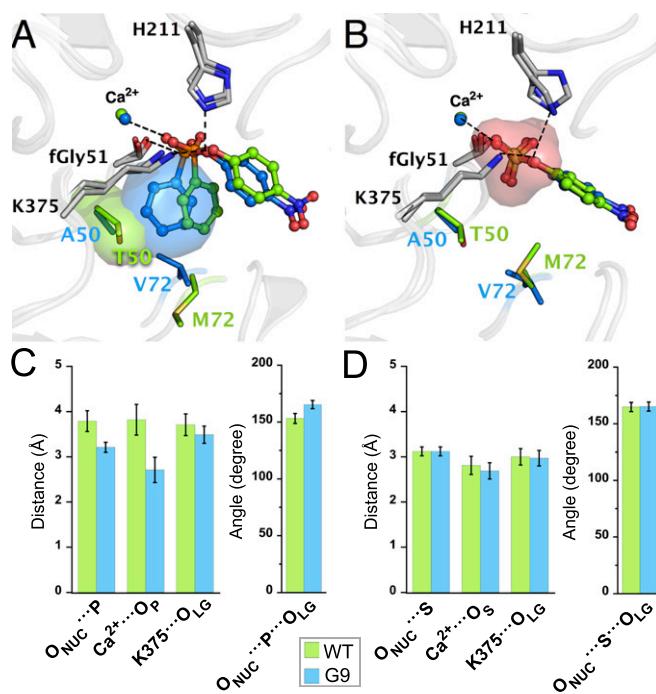


**Fig. 6.** Substrate repositioning induced by T50A and M72V in PAS<sup>G9</sup>. Representative stationary points from MD simulation for (A) phosphonate **2a** and (B) sulfate **1a** GS binding in PAS<sup>WT</sup> and PAS<sup>G9</sup>. (A) In PAS<sup>WT</sup> (green), the phenyl substituent of phosphonate **2a** constrains the GS in a compromised orientation for in-line nucleophilic attack, due to a clash with T50 (surface representation). In PAS<sup>G9</sup> (blue), T50A and M72V resolved the steric conflict and altered the original orientation with respect to fGly51, K375, and H211, leading to more efficient charge offset at the O<sub>LG</sub>. (B) In PAS<sup>WT</sup> (green), the GS of sulfate **1a** adopts a position with respect to K375 and H211 that stabilizes the negative charge building up on the O<sub>LG</sub>. However, MD simulations do not show significant repositioning of the sulfate **1a** GS after evolution in PAS<sup>G9</sup> (blue). (C and D) Evolution of the averaged distances (dotted lines in A and B) and angle (O<sub>NUC</sub>...P/S...O<sub>LG</sub>) between key residues and (C) phosphonate **2a** or (D) sulfate **1a** for nucleophilic attack (O<sub>NUC</sub>...P/S), metal coordination (Ca<sup>2+</sup>...O<sub>P/S</sub>), and general acid catalysis of the leaving group departure (K375...O<sub>LG</sub>). Distances are listed in *SI Appendix*, Table S8. Catalytic residues are shown as sticks and GS models as sticks and spheres and the metal ion as a sphere.

## Discussion

**The Energetic Cost of E•S Complex Formation Shapes Specificity More than the Nature of the TS in PAS.** The striking observation that none of the active-site residues previously implicated in catalysis (43, 47) were mutated, or even repositioned, raises the question of the changes in molecular recognition that have been brought about to achieve one of the largest rate enhancements observed in an evolution campaign ( $10^5$ -fold). Clues come from the features of PAS<sup>WT</sup>: The large energetic penalty observed for binding of phosphonates with “bulky” nonreacting side chains (e.g., phenyl in **2a** that, even by rotation, cannot easily be accommodated in the active site) suggests that steric factors govern its specificity. A lesser discrimination occurs between substrates with different charge and reaction mechanism, over substrates in which identical functional groups are cleaved: The chemically distinct phosphate mono- and diester (**4** vs. **3**) only differ by 50-fold in their  $k_{\text{cat}}/K_m$  values, but methyl- and phenylphosphonates (**2e** vs. **2a**) are turned over with a  $10^7$ -fold difference in  $k_{\text{cat}}/K_m$ . This phenomenon may be recurrent in the AP superfamily (48, 60). As a consequence, phenylphosphonate (**2a**) experiences only very poor leaving group stabilization in PAS<sup>WT</sup> (steep  $\beta_{\text{LG}}$ ), while the sterically less demanding methylphosphonate (**2e**) exhibits a shallower  $\beta_{\text{LG}}$ , pointing to a better fit and more efficient interactions with the departing phenolate. In the evolved PAS, the

deepening of the active site, which removed an original steric clash with the phenyl substituent of **2a**, was key to enhanced catalysis, by repositioning **2a** with respect to the catalytic center. This molecular solution to enzyme repurposing simply involves bringing the scissile functional group in a more favorable orientation for cleavage.

Fig. 7 illustrates a scenario where free-energy changes in evolution led to unlocking a previously disfavored (or inaccessible) binding orientation in the active site: The promiscuous substrate forms a Michaelis complex with the enzyme that is high in energy for both GS and TS ( $[E_{WT} \cdot S]_{Pn}$  and  $ES^{\ddagger}_{Pn}$ , blue), due to a misalignment with the catalytic core, which directly impairs phenylphosphonate hydrolysis (Fig. 7A). Similarly, suboptimal positioning of substrates in the phosphotriesterase OpdA (captured *in crystallo*) has been shown to compromise in-line nucleophile attack leading to a  $10^8$ -fold reduction in  $k_{cat}/K_m$  (61). However, in  $PAS^{G9}$ , mutations triggered a shift in substrate positioning, resulting in a better alignment, in terms of bond distances and angles, between the catalytic groups and the substrate center, at which electron density is located and charge changes occur, as the TS is approached. This amounts to lowering the energy of the newly evolved Michaelis complex ( $[E_{G9} \cdot S]_{Pn}$ ), and subsequently of TS ( $E_{G9}S^{\ddagger}_{Pn}$ ), while the native function sees the opposite trend (Fig. 7B). Evidence from phosphatase PP1 demonstrates that, like PAS, some active sites may be quite tolerant to fluctuations in the geometry of bound ligands; this tolerance may facilitate the catalysis of substrates whose positioning has been compromised by distinct steric requirements, both in the Michaelis complex and in the TS (56). These observations suggest that the ability of enzymes to accommodate substrates in multiple ways in one active site constitutes a mechanism of catalytic promiscuity (16, 62), akin to “differential ligand positioning” in antibodies (63).

**An Alternative Model for Rapid Functional Evolution in Promiscuous Enzymes.** Previous enzyme repurposing has been shown to involve mutations that—directly or via remote interactions—fine-tune the catalytic core, for example by metal displacement (24, 25), changes in water accessibility (64), the introduction of new catalytic residues (65), or the shift of a preexisting one (25), all of which impact interactions between enzyme and the TS. This matches textbook explanations of enzyme catalysis, focused on the place of bond making and breaking, where “ideal” enzyme–TS complementarity is to be achieved (66–69). However, in cases where catalytic residues were fully conserved, enzyme dynamics have been prominently discussed as facilitators of promiscuity, by enabling multiple scaffolds for the molecular recognition of distinct species or states (70–72). Such “conformational diversity” implies the coexistence of an ensemble of distinct active-site substates in equilibrium, in which a small fraction of conformers displays enhanced molecular interactions for the promiscuous substrate (73–76). As evolution proceeds, these minor, but lower-energy, promiscuous conformers were postulated to be enriched by “conformational selection” via an equilibrium shift (77, 78). Such features have indeed been shown to be adapted along an evolutionary trajectory (28, 79), although no direct link could be established between the promiscuous ligand and a given conformer.

Conformational changes are possible in PAS, but no evidence for their role in evolution was found: While we observe minor movements in surface loops, the position of the catalytic residues remains largely unaltered throughout evolution. Furthermore, the preexistence of a conformation in  $PAS^{WT}$  forming an “ideal fit” with phosphonate **2a** would lead to parallel Brønsted slopes in the evolved variants: The interactions would remain the same during evolution, but the fraction of productive conformers would increase (i.e., shift), resulting in an apparent increase in catalytic efficiency. Indeed such parallel Brønsted slopes were observed during the laboratory evolution of carbonic anhydrase II (80) and PTE (25). By contrast, the gradual changes in  $\beta_{LG}$  during evolution support the creation of a new distinct Michaelis complex that promotes better TS stabilization (shallower slope), rather than an equilibrium shift. Provided that the catalytic machinery is already

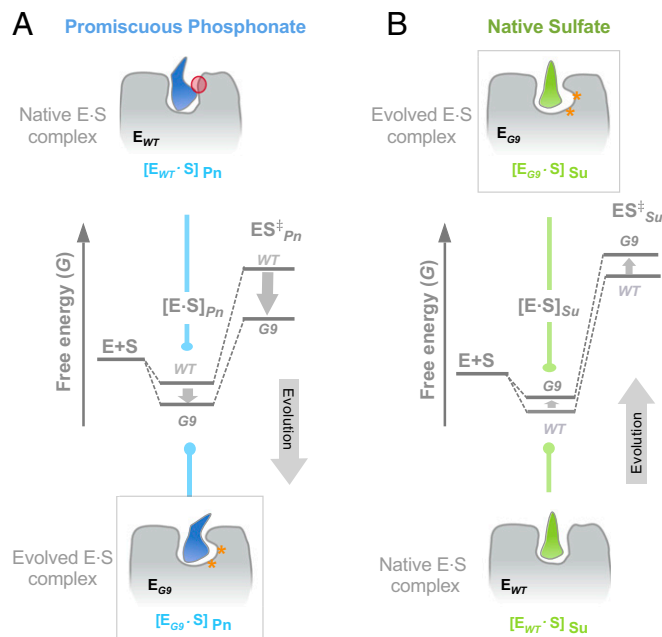


**Fig. 7.** Evolution creates a new Michaelis complex for the promiscuous ligand. Scheme representing the effect of evolution on the binding of (A) phosphonate **2a** and (B) sulfate **1a** in  $PAS^{WT}$  ( $E_{WT}$ ) and  $PAS^{G9}$  ( $E_{G9}$ ). (A) In  $E_{WT}$  (Top), the promiscuous phosphonate **2a** (blue) forms a distinct E•S complex with the enzyme ( $[E_{WT} \cdot S]_{Pn}$ ) compared with the native one (Bottom); the binding of the promiscuous ligand is constrained in a less productive orientation due to steric hindrance (red circle). Thus, both GS and TS complexes ( $[E_{WT} \cdot S]_{Pn}$  and  $E_{WT}S^{\ddagger}_{Pn}$ , respectively), have a high-energy state (Bottom). By reshaping the active site, evolution enhanced enzyme–substrate complementarity, for a more productive binding orientation, which lowered the energy state of the evolved  $[E_{G9} \cdot S]_{Pn}$  complex. The free energy (gray arrows) of the TS ( $E_{G9}S^{\ddagger}_{Pn}$ ) is lowered to a greater extent than the energy of the E•S complex, and differential binding of the TS over GS results in lower activation energy of  $k_{cat}/K_m$ . (B, Bottom) The native sulfate **1a** (green) forms a productive, low energy E•S complex ( $[E_{WT} \cdot S]_{Su}$ ) with the WT ( $E_{WT}$ ). In the evolved enzyme  $E_{G9}$  (B, Top), evolution may have compromised the binding of the native substrate, which could lead to an increase in the free energy of the  $[E_{G9} \cdot S]_{Su}$  complex, further amplified at the TS ( $E_{G9}S^{\ddagger}_{Su}$ ). Mutations are shown as orange asterisks.

in place and intrinsically efficient, contributions from conformational dynamics may not be necessary to achieve repurposing.

Our findings have implications for the molecular mechanism behind weak negative trade-offs, a commonly observed trend in directed evolution studies (17, 25, 81). Previously, weak trade-offs have been ascribed to intrinsic robustness of the native function (21) and/or to conformational selection, facilitated by gradual population shifts (78). The idea of intrinsic robustness has been recently challenged by evidence that stringent selection pressure would bias the fixation of mutations that promote weak trade-offs (82). In the evolution of PAS, conformational selection is unlikely (as discussed above). Instead, we hypothesize that the mutations leading to the formation of a new Michaelis complex with the promiscuous substrate are distinct from the residues coordinating the Michaelis complex of the native substrate (SI Appendix, Fig. S12). Hence, the trade-off between two activities will depend on the extent to which two substrates share common binding and catalytic features in the active site (32), that is, interconnected functional units (83), obviating the need for conformational diversity. In such cases, it becomes challenging to tailor efficient bispecificity (84, 85), or conversely to uncouple both functions to achieve exquisite specificity (83, 86), unless counterselection is applied.



**Functional Innovation in the AP Scaffold.** It is tempting to extrapolate the model described herein to a general mechanism in enzyme evolution: The tailoring of a Michaelis complex circumvents the need to “reinvent” functional groups for catalysis; instead, the existing machinery is deployed more efficiently via a limited set of mutations near to (but not in) the catalytic center (12). To some extent, this strategy reduces the problem of catalysis to a problem of binding (in terms of orientation and positioning of the substrate with respect to the catalytic center) (87). Thus, the “innovability” of the AP fold, that is, its ability to acquire new (catalytic) functions (88), may originate from two features of its active site: a well-organized and intrinsically reactive catalytic core (e.g., in PAS, a metal cofactor combined with nucleophile and general acids and bases) and a permissive binding region (89). The catalytic core can provide high (and thus less selective) reactivity to hydrolyze a broad range of chemical reactions, while the binding region governs the specificity. This active-site organization may be responsible for the broad catalytic diversity observed in highly promiscuous superfamilies (90, 91); for example, a recent study of a “pruned” AP scaffold, which only retains its reactive bimetallic core but lost all major interactions conferring specificity for phosphate mono- and diesters (34), demonstrated that a minimal “primordial” architecture (90, 92) remains reactive but can no longer discriminate between these substrates (33). As sequence space is traversed, the chances of encountering low-energy Michaelis complexes are higher than creating a catalytic arrangement *de novo*. This adaptive mechanism may provide a faster route toward catalytic efficiency and explain why promiscuous enzymes could be rapidly repurposed with a single substitution in several enzyme superfamilies (93, 94). Finally, our work may have important implications for enzyme engineering and design. We speculate that the high reactivity of PAS’s catalytic core may originate from its adaptation to a thermodynamically demanding reaction, sulfate transfer (59) (*SI Appendix, Table S1A*). Such a catalytic core may enable the turnover of less demanding substrates, thus illustrating a case of evolution in a thermodynamically “downward” direction toward “easier” reactions. Starting evolution from highly reactive catalytic centers, able to perform the most thermodynamically demanding reactions, could inform strategies to engineer and design new catalysts for a broad range of applications.

## Materials and Methods

Detailed materials and methods are provided in *SI Appendix*.

- Mohamed MF, Hollfelder F (2013) Efficient, crosswise catalytic promiscuity among enzymes that catalyze phosphoryl transfer. *Biochim Biophys Acta* 1834:417–424.
- Huang H, et al. (2015) Panoramic view of a superfamily of phosphatases through substrate profiling. *Proc Natl Acad Sci USA* 112:E1974–E1983.
- Copley SD (2003) Enzymes with extra talents: Moonlighting functions and catalytic promiscuity. *Curr Opin Chem Biol* 7:265–272.
- Hult K, Berglund P (2007) Enzyme promiscuity: Mechanism and applications. *Trends Biotechnol* 25:231–238.
- Schulenburg C, Miller BG (2014) Enzyme recruitment and its role in metabolic expansion. *Biochemistry* 53:836–845.
- Jensen RA (1976) Enzyme recruitment in evolution of new function. *Annu Rev Microbiol* 30:409–425.
- Leong BJ, Last RL (2017) Promiscuity, impersonation and accommodation: Evolution of plant specialized metabolism. *Curr Opin Struct Biol* 47:105–112.
- Soo VWC, Hanson-Manful P, Patrick WM (2011) Artificial gene amplification reveals an abundance of promiscuous resistance determinants in *Escherichia coli*. *Proc Natl Acad Sci USA* 108:1484–1489.
- Yip SH-C, Matsumura I (2013) Substrate ambiguous enzymes within the *Escherichia coli* proteome offer different evolutionary solutions to the same problem. *Mol Biol Evol* 30:2001–2012.
- Miller BG, Raines RT (2005) Reconstitution of a defunct glycolytic pathway via recruitment of ambiguous sugar kinases. *Biochemistry* 44:10776–10783.
- Renata H, Wang ZJ, Arnold FH (2015) Expanding the enzyme universe: Accessing non-rare reactions by mechanism-guided directed evolution. *Angew Chem Int Ed Engl* 54:3351–3367.
- O’Brien PJ, Herschlag D (1999) Catalytic promiscuity and the evolution of new enzymatic activities. *Chem Biol* 6:R91–R105.
- Brown DW, Schaab MR, Birmingham WR, Armstrong RN (2009) Evolution of the antibiotic resistance protein, FosA, is linked to a catalytically promiscuous progenitor. *Biochemistry* 48:1847–1849.
- Weng J-K, Philippe RN, Noel JP (2012) The rise of chemodiversity in plants. *Science* 336:1667–1670.
- Copley SD (2009) Evolution of efficient pathways for degradation of anthropogenic chemicals. *Nat Chem Biol* 5:559–566.
- Nobeli I, Favia AD, Thornton JM (2009) Protein promiscuity and its implications for biotechnology. *Nat Biotechnol* 27:157–167.
- Khersonsky O, Tawfik DS (2010) Enzyme promiscuity: A mechanistic and evolutionary perspective. *Annu Rev Biochem* 79:471–505.
- Fasan R, Meharena YT, Snow CD, Poulos TL, Arnold FH (2008) Evolutionary history of a specialized p450 propane monooxygenase. *J Mol Biol* 383:1069–1080.
- Boucher JI, Jacobowitz JR, Beckett BC, Classen S, Theobald DL (2014) An atomic-resolution view of neofunctionalization in the evolution of apicomplexan lactate dehydrogenases. *eLife* 3:e02304.
- Newton MS, et al. (2017) Structural and functional innovations in the real-time evolution of new ( $\beta\alpha\alpha$ ) barrel enzymes. *Proc Natl Acad Sci USA* 114:4727–4732.
- Aharoni A, et al. (2005) The ‘evolubility’ of promiscuous protein functions. *Nat Genet* 37:73–76.
- Huang R, et al. (2012) Enzyme functional evolution through improved catalysis of ancestrally nonpreferred substrates. *Proc Natl Acad Sci USA* 109:2966–2971.
- Miton CM, Tokuriki N (2016) How mutational epistasis impairs predictability in protein evolution and design. *Protein Sci* 25:1260–1272.
- Ben-David M, et al. (2013) Catalytic metal ion rearrangements underline promiscuity and evolvability of a metalloenzyme. *J Mol Biol* 425:1028–1038.
- Tokuriki N, et al. (2012) Diminishing returns and tradeoffs constrain the laboratory optimization of an enzyme. *Nat Commun* 3:1257.
- Wang X, Minasov G, Shoichet BK (2002) The structural bases of antibiotic resistance in the clinically derived mutant beta-lactamases TEM-30, TEM-32, and TEM-34. *J Biol Chem* 277:32149–32156.
- Sykora J, et al. (2014) Dynamics and hydration explain failed functional transformation in dehalogenase design. *Nat Chem Biol* 10:428–430.

28. Campbell E, et al. (2016) The role of protein dynamics in the evolution of new enzyme function. *Nat Chem Biol* 12:944–950.
29. Meier MM, et al. (2013) Molecular engineering of organophosphate hydrolysis activity from a weak promiscuous lactonase template. *J Am Chem Soc* 135:11670–11677.
30. Kaltenbach M, Jackson CJ, Campbell EC, Hofffelder F, Tokuriki N (2015) Reverse evolution leads to genotypic incompatibility despite functional and active site convergence. *eLife* 4:e06492.
31. Jacob F (1977) Evolution and tinkering. *Science* 196:1161–1166.
32. Babbie A, Tokuriki N, Hofffelder F (2010) What makes an enzyme promiscuous? *Curr Opin Chem Biol* 14:200–207.
33. Sundén F, et al. (2017) Differential catalytic promiscuity of the alkaline phosphatase superfamily bimetallo core reveals mechanistic features underlying enzyme evolution. *J Biol Chem* 292:20960–20974.
34. Sundén F, et al. (2016) Mechanistic and evolutionary insights from comparative enzymology of phosphomonoesterases and phosphodiesterases across the alkaline phosphatase superfamily. *J Am Chem Soc* 138:14273–14287.
35. Andrews LD, Zalatan JG, Herschlag D (2014) Probing the origins of catalytic discrimination between phosphate and sulfate monoester hydrolysis: Comparative analysis of alkaline phosphatase and protein tyrosine phosphatases. *Biochemistry* 53:6811–6819.
36. Wiersma-Koch H, Sundén F, Herschlag D (2013) Site-directed mutagenesis maps interactions that enhance cognate and limit promiscuous catalysis by an alkaline phosphatase superfamily phosphodiesterase. *Biochemistry* 52:9167–9176.
37. Jonas S, Hofffelder F (2009) Mapping catalytic promiscuity in the alkaline phosphatase superfamily. *Pure Appl Chem* 81:731–742.
38. Nikolic-Hughes I, Rees DC, Herschlag D (2004) Do electrostatic interactions with positively charged active site groups tighten the transition state for enzymatic phosphoryl transfer? *J Am Chem Soc* 126:11814–11819.
39. Hofffelder F, Herschlag D (1995) The nature of the transition state for enzyme-catalyzed phosphoryl transfer. Hydrolysis of O-aryl phosphorothioates by alkaline phosphatase. *Biochemistry* 34:12255–12264.
40. Cleland WW, Hengge AC (2006) Enzymatic mechanisms of phosphate and sulfate transfer. *Chem Rev* 106:3252–3278.
41. Lassila JK, Zalatan JG, Herschlag D (2011) Biological phosphoryl-transfer reactions: Understanding mechanism and catalysis. *Annu Rev Biochem* 80:669–702.
42. Zalatan JG, Herschlag D (2006) Alkaline phosphatase mono- and diesterase reactions: Comparative transition state analysis. *J Am Chem Soc* 128:1293–1303.
43. Boltes I, et al. (2001) 1.3 Å structure of arylsulfatase from *Pseudomonas aeruginosa* establishes the catalytic mechanism of sulfate ester cleavage in the sulfatase family. *Structure* 9:483–491.
44. Dierks T, et al. (1998) Posttranslational formation of formylglycine in prokaryotic sulfatases by modification of either cysteine or serine. *J Biol Chem* 273:25560–25564.
45. Beil S, et al. (1995) Purification and characterization of the arylsulfatase synthesized by *Pseudomonas aeruginosa* PAO during growth in sulfate-free medium and cloning of the arylsulfatase gene (*atsA*). *Eur J Biochem* 229:385–394.
46. Kintses B, et al. (2012) Picoliter cell lysate assays in microfluidic droplet compartments for directed enzyme evolution. *Chem Biol* 19:1001–1009.
47. Olguin LF, Askew SE, O'Donoghue AC, Hofffelder F (2008) Efficient catalytic promiscuity in an enzyme superfamily: An arylsulfatase shows a rate acceleration of  $10^{13}$  for phosphate monoester hydrolysis. *J Am Chem Soc* 130:16547–16555.
48. Babbie AC, Bandyopadhyay S, Olguin LF, Hofffelder F (2009) Efficient catalytic promiscuity for chemically distinct reactions. *Angew Chem Int Ed Engl* 48:3692–3694.
49. Hanson SR, Best MD, Wong C-H (2004) Sulfatases: Structure, mechanism, biological activity, inhibition, and synthetic utility. *Angew Chem Int Ed Engl* 43:5736–5763.
50. Appel MJ, Bertozzi CR (2015) Formylglycine, a post-translationally generated residue with unique catalytic capabilities and biotechnology applications. *ACS Chem Biol* 10:72–84.
51. Bershtein S, Goldin K, Tawfik DS (2008) Intense neutral drifts yield robust and evolvable consensus proteins. *J Mol Biol* 379:1029–1044.
52. Bloom JD, Romero PA, Lu Z, Arnold FH (2007) Neutral genetic drift can alter promiscuous protein functions, potentially aiding functional evolution. *Biol Direct* 2:17.
53. van Loo B, et al. (2018) Transition state interactions in a promiscuous enzyme: sulfate and phosphate monoester hydrolysis by *Pseudomonas aeruginosa* arylsulfatase. [bioRxiv:10.1101/327643](https://doi.org/10.1101/327643).
54. Gang DR, et al. (2002) Characterization of phenylpropene O-methyltransferases from sweet basil: Facile change of substrate specificity and convergent evolution within a plant O-methyltransferase family. *Plant Cell* 14:505–519.
55. McWhirter C, et al. (2008) Mechanistic study of protein phosphatase-1 (PP1), a catalytically promiscuous enzyme. *J Am Chem Soc* 130:13673–13682.
56. Chu Y, Williams NH, Hengge AC (2017) Transition states and control of substrate preference in the promiscuous phosphatase PP1. *Biochemistry* 56:3923–3933.
57. O'Brien PJ, Herschlag D (1999) Does the active site arginine change the nature of the transition state for alkaline phosphatase-catalyzed phosphoryl transfer? *J Am Chem Soc* 121:11022–11023.
58. Furnham N, et al. (2012) Exploring the evolution of novel enzyme functions within structurally defined protein superfamilies. *PLoS Comput Biol* 8:e1002403.
59. Edwards DR, Lohman DC, Wolfenden R (2012) Catalytic proficiency: The extreme case of S-O cleaving sulfatases. *J Am Chem Soc* 134:525–531.
60. Bayer CD, van Loo B, Hofffelder F (2017) Specificity effects of amino acid substitutions in promiscuous hydrolases: Context-dependence of catalytic residue contributions to local fitness landscapes in nearby sequence space. *ChemBioChem* 18:1001–1015.
61. Jackson CJ, et al. (2008) *In crystallo* capture of a Michaelis complex and product-binding modes of a bacterial phosphotriesterase. *J Mol Biol* 375:1189–1196.
62. Ekroos M, Sjögren T (2006) Structural basis for ligand promiscuity in cytochrome P450 3A4. *Proc Natl Acad Sci USA* 103:13682–13687.
63. Mariuzza RA (2006) Multiple paths to multispecificity. *Immunity* 24:359–361.
64. Czerwinski RM, Harris TK, Massiah MA, Mildvan AS, Whitman CP (2001) The structural basis for the perturbed pKa of the catalytic base in 4-oxalocrotonate tautomerase: Kinetic and structural effects of mutations of Phe-50. *Biochemistry* 40:1984–1995.
65. Obexer R, et al. (2017) Emergence of a catalytic tetrad during evolution of a highly active artificial aldolase. *Nat Chem* 9:50–56.
66. Blomberg R, et al. (2013) Precision is essential for efficient catalysis in an evolved Kemp eliminase. *Nature* 503:418–421.
67. Fersht AR (1974) Catalysis, binding and enzyme-substrate complementarity. *Proc R Soc Lond B Biol Sci* 187:397–407.
68. Jogl G, Rozovsky S, McDermott AE, Tong L (2003) Optimal alignment for enzymatic proton transfer: Structure of the Michaelis complex of triosephosphate isomerase at 1.2-Å resolution. *Proc Natl Acad Sci USA* 100:50–55.
69. Preiswerk N, et al. (2014) Impact of scaffold rigidity on the design and evolution of an artificial Diels-Alderase. *Proc Natl Acad Sci USA* 111:8013–8018.
70. Henzler-Wildman K, Kern D (2007) Dynamic personalities of proteins. *Nature* 450:964–972.
71. Honaker MT, Acchione M, Sumida JP, Atkins WM (2011) Ensemble perspective for catalytic promiscuity: Calorimetric analysis of the active site conformational landscape of a detoxification enzyme. *J Biol Chem* 286:42770–42776.
72. Campbell EC, et al. (2017) Laboratory evolution of protein conformational dynamics. *Curr Opin Struct Biol* 50:49–57.
73. Rader SD, Agard DA (1997) Conformational substates in enzyme mechanism: The 120 K structure of alpha-lytic protease at 1.5 Å resolution. *Protein Sci* 6:1375–1386.
74. Boehr DD, Nussinov R, Wright PE (2009) The role of dynamic conformational ensembles in biomolecular recognition. *Nat Chem Biol* 5:789–796.
75. Ma B, Nussinov R (2010) Enzyme dynamics point to stepwise conformational selection in catalysis. *Curr Opin Chem Biol* 14:652–659.
76. Benkovic SJ, Hammes GG, Hammes-Schiffer S (2008) Free-energy landscape of enzyme catalysis. *Biochemistry* 47:3317–3321.
77. Tokuriki N, Tawfik DS (2009) Protein dynamism and evolvability. *Science* 324:203–207.
78. James LC, Tawfik DS (2003) Conformational diversity and protein evolution—A 60-year-old hypothesis revisited. *Trends Biochem Sci* 28:361–368.
79. Mabbitt PD, et al. (2016) Conformational disorganization within the active site of a recently evolved organophosphate hydrolase limits its catalytic efficiency. *Biochemistry* 55:1408–1417.
80. Gould SM, Tawfik DS (2005) Directed evolution of the promiscuous esterase activity of carbonic anhydrase II. *Biochemistry* 44:5444–5452.
81. Matsumura I, Ellington AD (2001) In vitro evolution of beta-glucuronidase into a beta-galactosidase proceeds through non-specific intermediates. *J Mol Biol* 305:331–339.
82. Kaltenbach M, Emond S, Hofffelder F, Tokuriki N (2016) Functional trade-offs in promiscuous enzymes cannot be explained by intrinsic mutational robustness of the native activity. *PLoS Genet* 12:e1006305.
83. Sundén F, Peck A, Salzman J, Ressler S, Herschlag D (2015) Extensive site-directed mutagenesis reveals interconnected functional units in the alkaline phosphatase active site. *eLife* 4:e06181.
84. Sugrue E, Scott C, Jackson CJ (2017) Constrained evolution of a bispecific enzyme: Lessons for biocatalyst design. *Org Biomol Chem* 15:937–946.
85. Khanal A, Yu McLoughlin S, Kershner JP, Copley SD (2015) Differential effects of a mutation on the normal and promiscuous activities of orthologs: Implications for normal and directed evolution. *Mol Biol Evol* 32:100–108.
86. Vorobieva AA, Khan MS, Soumillion P (2014) *Escherichia coli* D-malate dehydrogenase, a generalist enzyme active in the leucine biosynthesis pathway. *J Biol Chem* 289:29086–29096.
87. Kirby AJ, Hofffelder F (2009) *From Enzyme Models to Model Enzymes* (Royal Society of Chemistry, Cambridge, UK).
88. Wagner A (2011) *The Origins of Evolutionary Innovations* (Oxford Univ Press, Oxford).
89. Fong DH, Berghuis AM (2002) Substrate promiscuity of an aminoglycoside antibiotic resistance enzyme via target mimicry. *EMBO J* 21:2323–2331.
90. Pandya C, Farrell JD, Dunaway-Mariano D, Allen KN (2014) Enzyme promiscuity: Engine of evolutionary innovation. *J Biol Chem* 289:30229–30236.
91. Vick JE, Gerlt JA (2007) Evolutionary potential of (beta/alpha)<sub>8</sub>-barrels: Stepwise evolution of a “new” reaction in the enolase superfamily. *Biochemistry* 46:14589–14597.
92. Toscano MD, Woycechowsky KJ, Hilvert D (2007) Minimalist active-site redesign: Teaching old enzymes new tricks. *Angew Chem Int Ed Engl* 46:3212–3236.
93. Schmidt DMZ, et al. (2003) Evolutionary potential of (beta/alpha)<sub>8</sub>-barrels: Functional promiscuity produced by single substitutions in the enolase superfamily. *Biochemistry* 42:8387–8393.
94. McLoughlin SY, Copley SD (2008) A compromise required by gene sharing enables survival: Implications for evolution of new enzyme activities. *Proc Natl Acad Sci USA* 105:13497–13502.
95. Zaccolo M, Williams DM, Brown DM, Gherardi E (1996) An approach to random mutagenesis of DNA using mixtures of triphosphate derivatives of nucleoside analogues. *J Mol Biol* 255:589–603.
96. Arnold FH, Georgiou G (2003) *Directed Evolution Library Creation* (Humana, New York).
97. Jorgensen WL, Maxwell DS, Tirado-Rives J (1996) Development and testing of the OPLS all-atom force field on conformational energetics and properties of organic liquids. *J Am Chem Soc* 118:11225–11236.
98. Jorgensen WL, Chandrasekhar J, Madura JD, Impey RW, Klein ML (1983) Comparison of simple potential functions for simulating liquid water. *J Chem Phys* 79:926–935.
99. Marelis J, Kolmodin K, Feiberger I, Aqvist J (1998) Q: A molecular dynamics program for free energy calculations and empirical valence bond simulations in biomolecular systems. *J Mol Graph Model* 16:213–225.